Electronic Supplementary Information

Electronic delocalization in charged macrocycles is associated with global aromaticity

David Bradley, Bethany K. Hillier and Martin D. Peeks*

School of Chemistry, University of New South Wales, Sydney NSW 2052 Australia

* Corresponding author: m.peeks@unsw.edu.au

Contents

S1. Computational details

All DFT calculations were completed with Gaussian16.[1] The geometry of *c*-**P6•T6** was optimized at each charge and DFT functional combination (BLYP, B1LYP, BLYP35, BHandHLYP) [2–5] with the 6-31G* basis set.[6–9] We were however unable to optimize *c*-**P6•T6**$^{4+}$ at the BLYP level, so we included LC-ωHPBE[10] (ω = 0.1) and CAM-B3LYP[11] calculations to sufficiently investigate IFDIs. The CAM-B3LYP geometry was taken from the literature.[12] We examined *c*-**P6•T6**$^{6+}$ more extensively by including B3LYP,[13,14] M06-2X,[15] CAM-B3LYP, and LC-ωHPBE (ω = 0.1) calculations. Calculations at the B3LYP and CAM-B3LYP level included Grimme's D3 dispersion correction.[16] We replaced the trihexylsilyl solubilization groups with hydrogen atoms, such that each porphyrin subunit contains two phenyl groups. NMR chemical shifts, which are used in the calculation of ring current susceptibilities, were calculated at each functional with the polarization continuum model (dichloromethane as solvent).

Ring current geometric factors (RCGFs) were calculated for each oxidation state and each DFT functional using a MATLAB script which can be found in the repository (https://github.com/mjirasek/Local_vs_Global_RMC). Using these RCGFs, we calculated local and global ring current susceptibilities (called I/B_{local} and I/B_{global}) for each oxidation state and DFT functional combination according to the multiple current loop model.[17]

Delocalization indices were calculated using Multiwfn[18] from formatted checkpoint files. We also calculated delocalization indices with AIMAll Pro (version 19.10.12)[19] and found no significant difference in conclusions between the two packages. We define "fragments" as porphyrin subunits in *c*-**P6•T6** and benzene subunits in [8]CPP. We investigated the effect of including alkyne fragments in our definition of fragments for *c*-**P6•T6** – see SI section S2. In several plots we depict the IFDI values between monomer subunits as matrices. In these plots we have set the diagonal elements, which correspond to "localization indices" (*i.e.* the number of electrons localized to a monomer subunit), to zero for clarity.

S2. Effect of including alkyne groups in fragments for IFDI
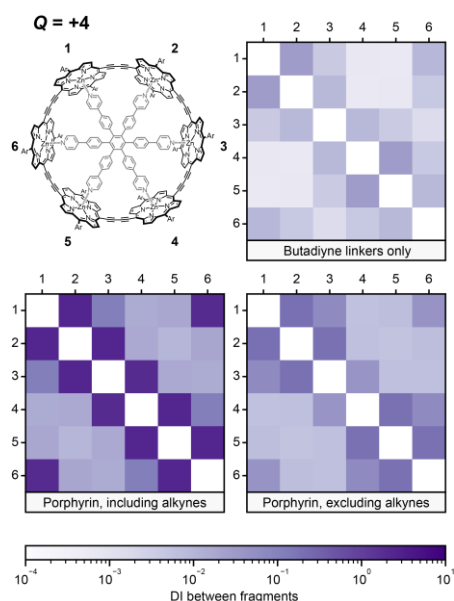
Figure S1 Comparison of delocalization index (DI) between subunits in *c*-P6•T6^{4+} at the BLYP35 level.

For the calculations of IFDIs we tested three definitions of the "fragment":

- Butadiyne linkers only, where each fragment is defined as the four carbon atoms between a set of porphyrin subunits.
- Porphyrin subunits, where each fragment is defined as only atoms that make up each porphyrin, excluding hydrogens and phenyl sidegroups.
- Porphyrin and alkyne groups, where each fragment is defined as the atoms that make up the porphyrin subunits and two carbon atoms (i.e., acetylene fragment) from each side of the porphyrin.

Including the alkyne groups in the fragments increases the IFDI, but does not change the conclusions. Whether or not the alkynes are included, the IFDI$_{opp}$ values (a) reflect the global (anti)aromaticity of the molecules, and (b) vary proportionally to the I/B_{global} when the %HF in the DFT functional is changed.

.

S3. Relationship between IFDI and %HF
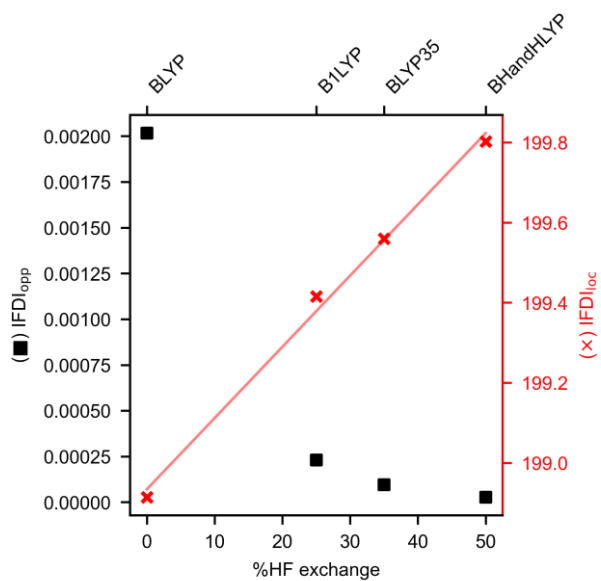
Figure S2 Relationship between IFDI and %HF in *c*-**P6•T6**.
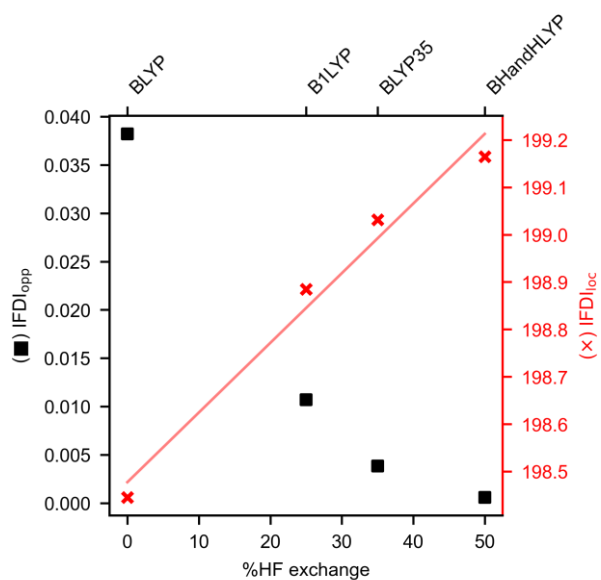
Figure S3 Relationship between IFDI and %HF in *c*-**P6•T6**$^{2+}$.
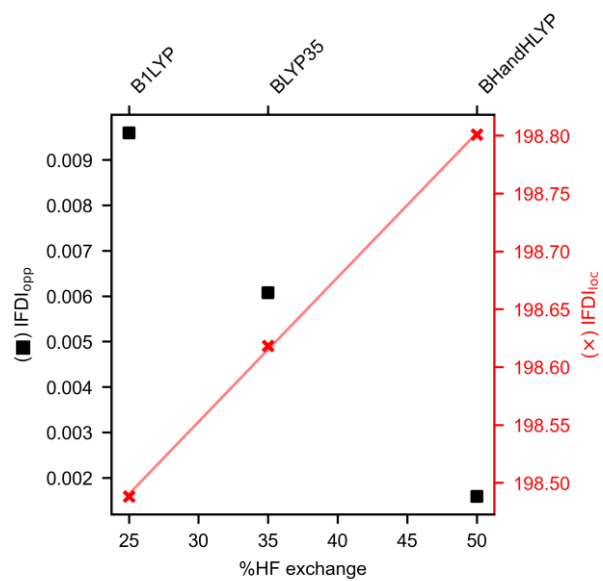
Figure S4 Relationship between IFDI and %HF in c-**P6•T6**$^{4+}$.
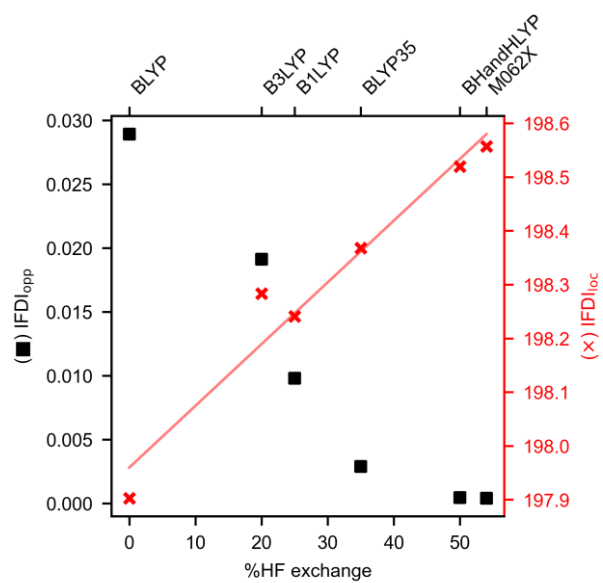
Figure S5 Relationship between IFDI and %HF in c-**P6•T6**$^{6+}$.
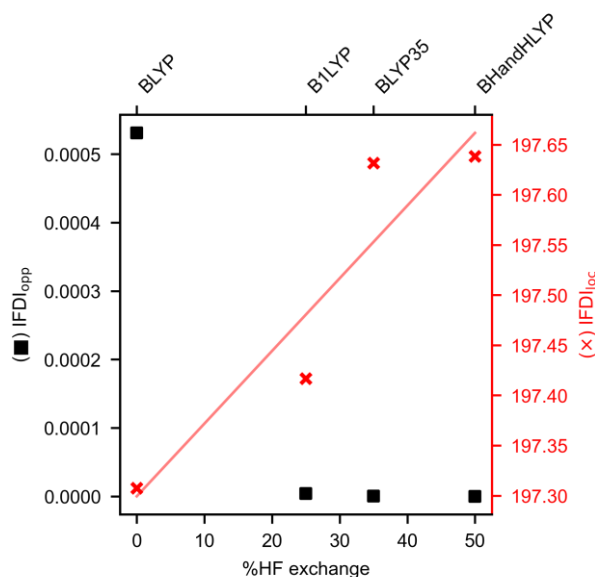
Figure S6 Relationship between IFDI values (IFDI$_{opp}$, left, and IFDI$_{loc}$, right) and %HF in ***c*-P6•T6**$^{12+}$.

Table S1 Fitting parameters of the relationships between IFDI$_{opp}$ and the global ring current susceptibility, I/B_{global}, and between IFDI$_{loc}$ and %HF.

		***Q* = 0**	***Q* = +2**	***Q* = +4**	***Q* = +6**	***Q* = +12**
	IFDI$_{opp}$[a]	9.5×10^{-5}	0.0038	0.0061	0.0029	7.0×10^{-8}
IFDI$_{opp}$ vs *I/B*	Gradient	4572	−1611	17262	−2554	−86920
	Intercept	−0.21	0.05	−26.85	−0.05	1.01
	R^2	>0.999	>0.999	0.959	>0.999	>0.999[b]
IFDI$_{loc}$ vs %HF	Gradient	0.018	0.015	0.012	0.011	0.007
	Intercept	198.9	198.5	198.2	198.0	197.3
	R^2	0.995	0.978	>0.999	0.954	0.865

[a] These IFDI$_{opp}$ values refer to those calculated at the BLYP35 level. [b] The R^2 value for Q = +12 is much reduced if the outlying BLYP value is excluded from the fit, and becomes 0.871; the data are plotted in figure S16.

The calculated delocalization indices for ***c*-P6•T6**^{Q} (Q = 0, +2, +4, +6, +12) depend significantly on the amount of Hartree-Fock (HF) exchange in the DFT functional. This parameter is commonly associated with inaccuracies in DFT calculations – electron delocalization tends to be exaggerated in functionals with low HF exchange, whereas delocalization is minimized in those with high HF exchange. In systems such as porphyrin nanorings, the amount of HF exchange essentially determines whether the nanoring is globally or locally aromatic (according to the magnetic criteria based on NMR chemical shifts).

IFDI$_{loc}$ values, which can be thought of as an electron localization index for the porphyrin subunits, generally follow a linear relationship with %HF in the BLYP, B1LYP, BLYP35, and BHandHLYP series in all oxidation states. This trend is reversed in IFDI$_{opp}$ calculations, in which high amounts of HF exchange decrease the number of shared electrons between opposite fragments.

S4. Additional matrix figures for *c*-P6•T6
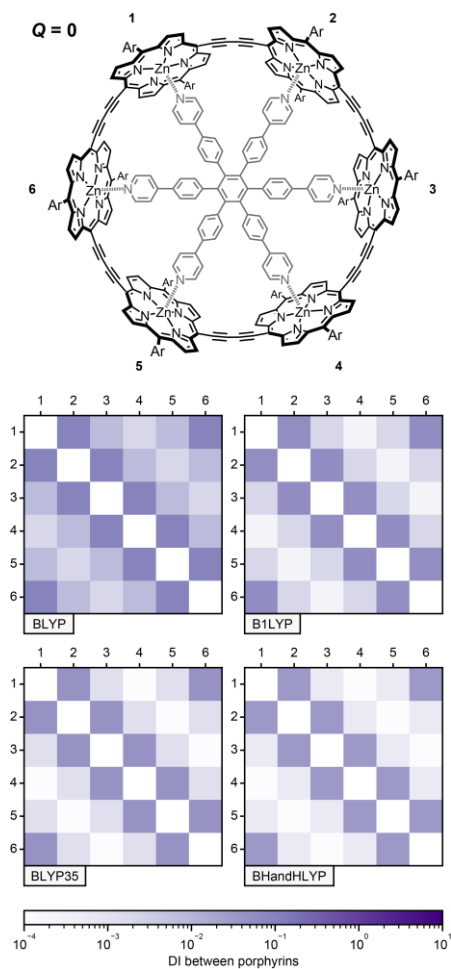
Figure S7 Delocalization matrices for *c*-P6•T6 using various functionals.
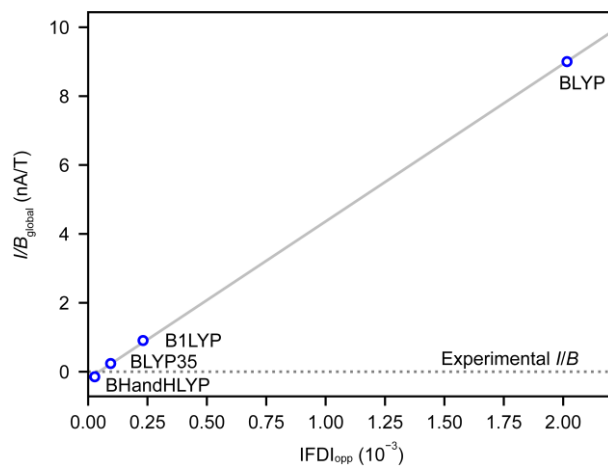
Figure S8 $IFDI_{opp}$ *vs* I/B_{global} for *c*-P6•T6 with different DFT functionals. The dotted line corresponds to the I/B_{global} determined from the experimental NMR spectrum.
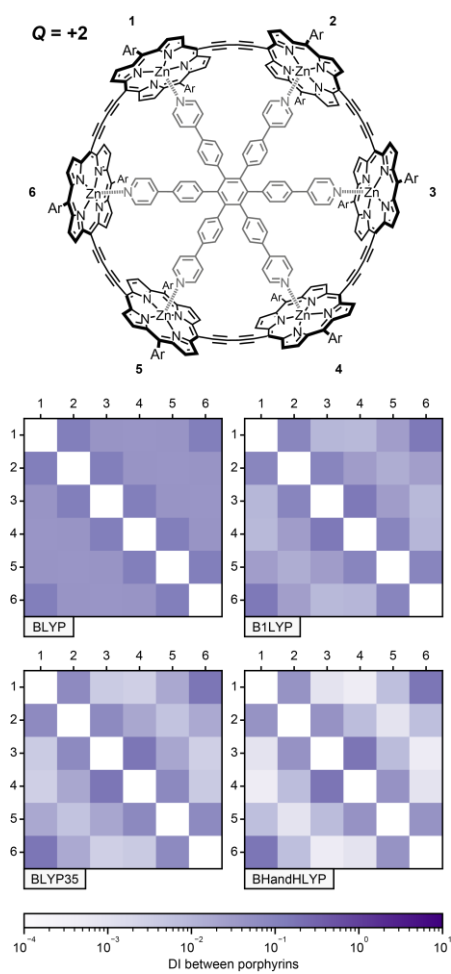
Figure S9 Delocalization matrices for *c*-P6•T6^{2+} with various functionals.
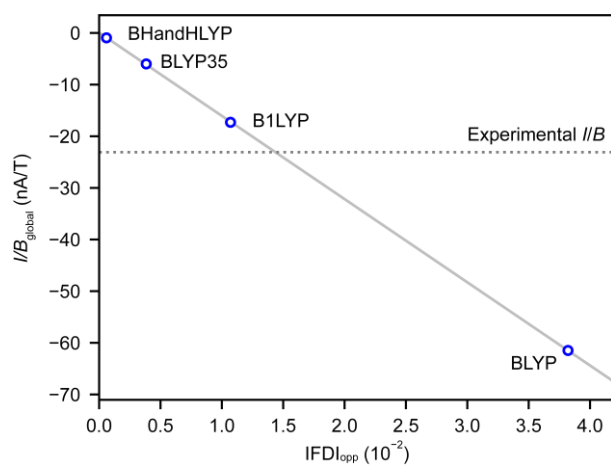
Figure S10 IFDI$_{opp}$ *vs* I/B$_{global}$ for *c*-P6•T6^{2+} with different DFT functionals. The dotted line corresponds to the I/B$_{global}$ determined from the experimental NMR spectrum.
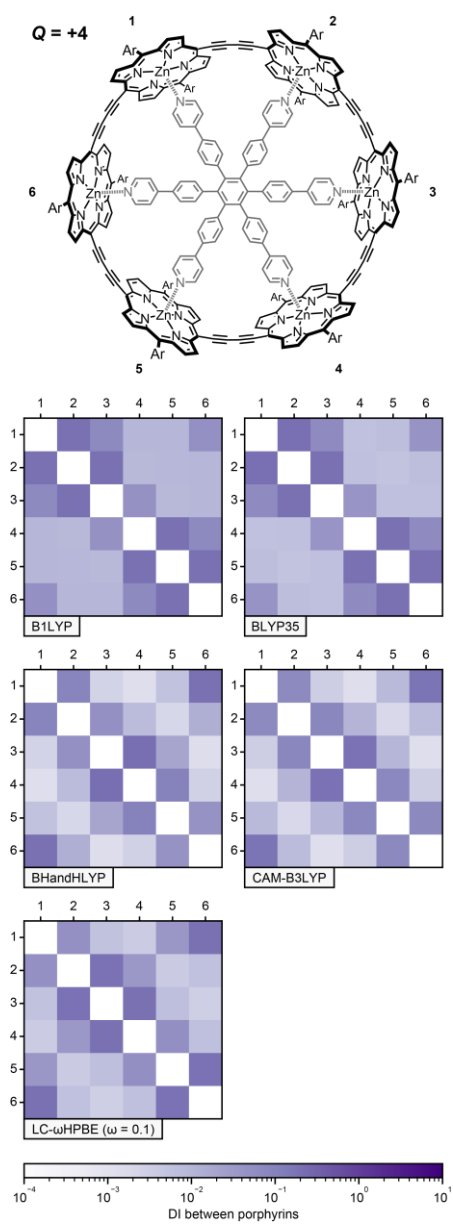
Figure S11 Delocalization matrices for *c*-P6•T6^{4+} with various functionals.
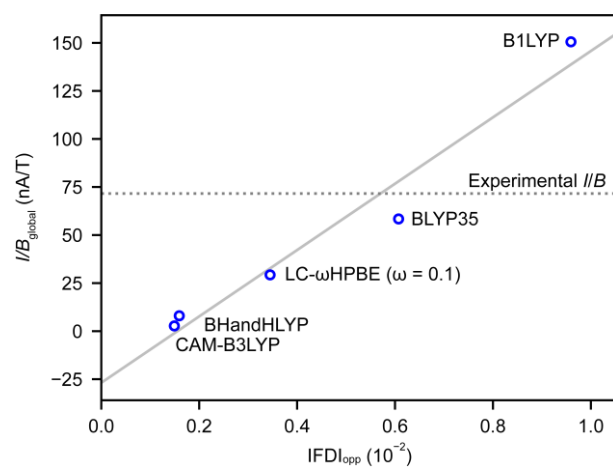
Figure S12 IFDI$_{opp}$ *vs* I/B$_{global}$ for **c-P6•T6**[4+] with different DFT functionals. The dotted line corresponds to the I/B$_{global}$ determined from the experimental NMR spectrum.
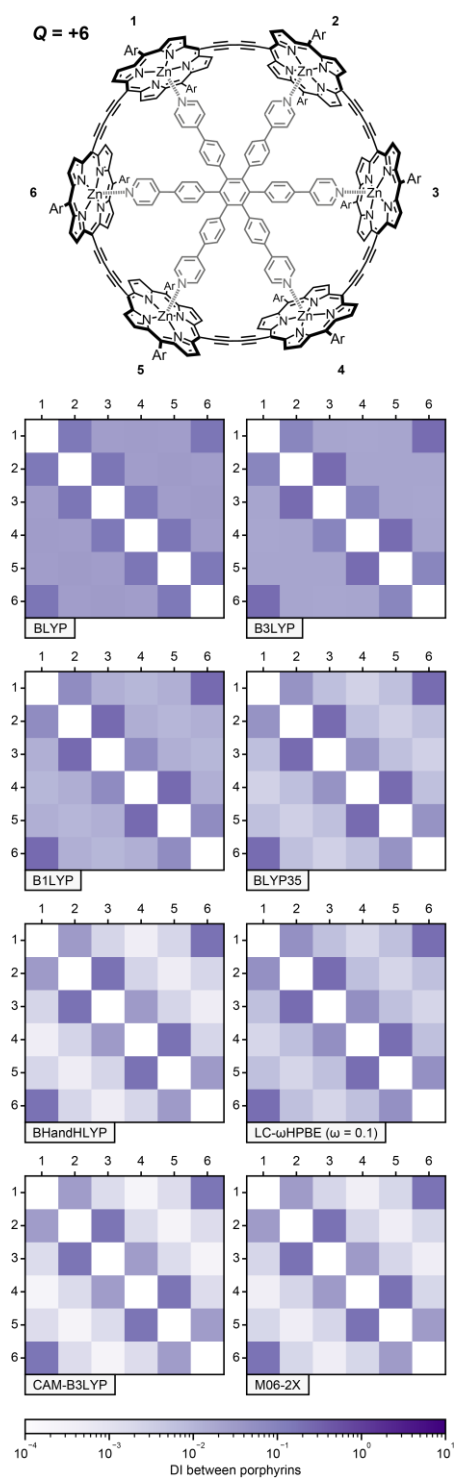
Figure S13 Delocalization matrices for *c*-P6•T6[6+] with various functionals.
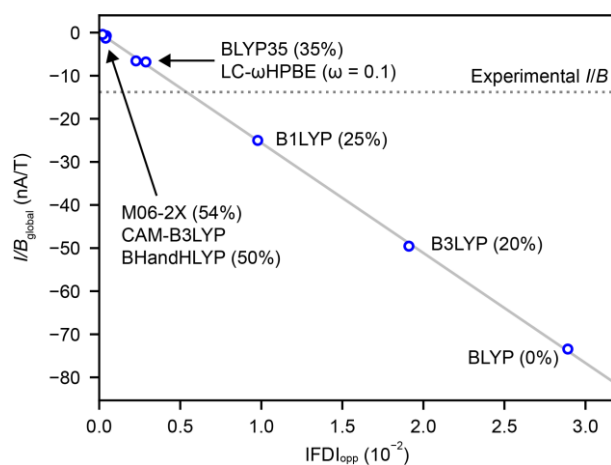
Figure S14 IFDI$_{opp}$ *vs* I/B$_{global}$ for *c*-P6•T6^{6+} with different DFT functionals. The dotted line corresponds to the I/B$_{global}$ determined from the experimental NMR spectrum.
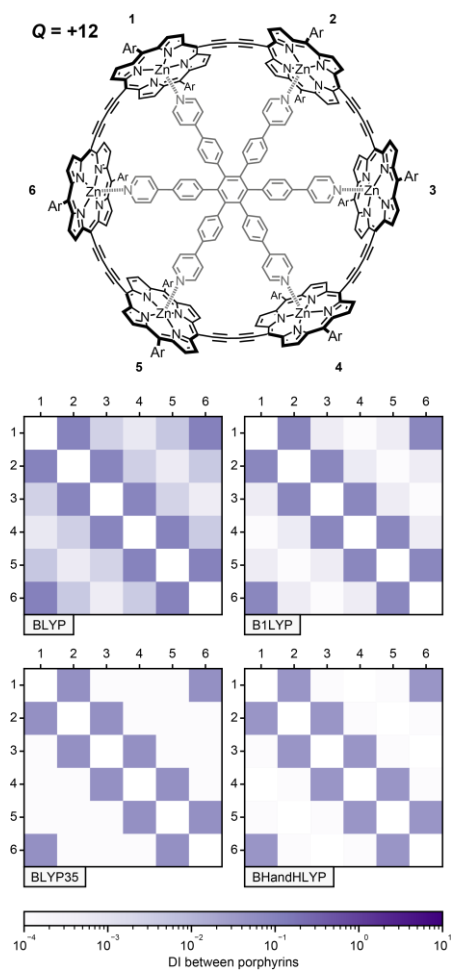
Figure S15 Delocalization matrices for *c*-P6•T6^{12+} with various functionals.
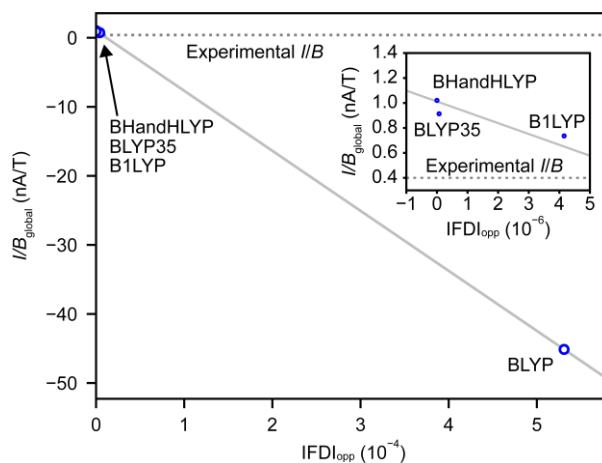
Figure S16 IFDI$_{opp}$ *vs* I/B_{global} for c-**P6•T6**$^{12+}$ with different DFT functionals. The dotted line corresponds to the I/B_{global} determined from the experimental NMR spectrum. The inset shows an expansion of the low I/B and IFDI$_{opp}$ region.
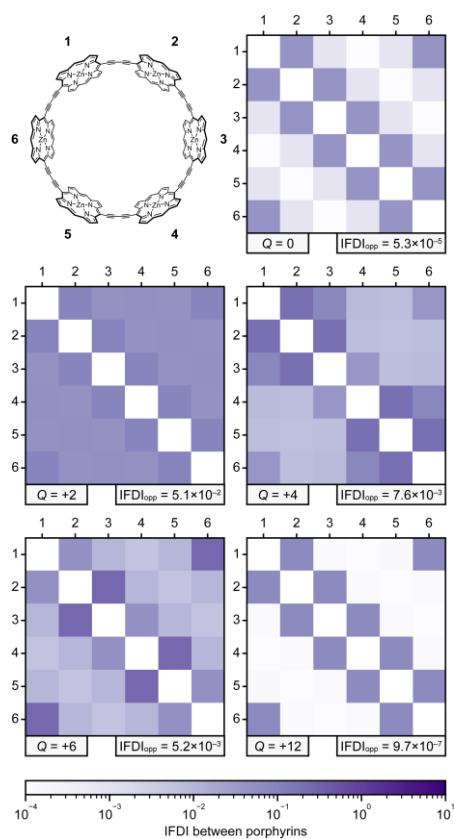
Figure S17 Matrices of IFDI values between fragments in c-**P6**^{Q}, i.e. the nanoring without the central hexapyridyl template. The mean IFDI between opposite porphyrins, as the fragment analogue of PDI, is reported as IFDI$_{opp}$. Calculated at the BLYP35/6-31G* level.

S5. Additional matrix figures for [8]CPP
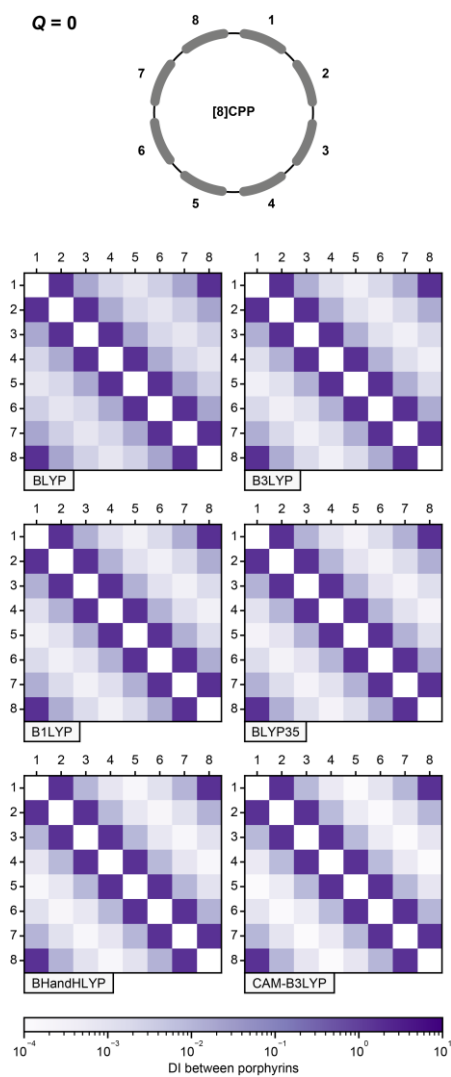
Figure S18 IFDI values between phenyl fragments in [8]CPP with various DFT functionals.
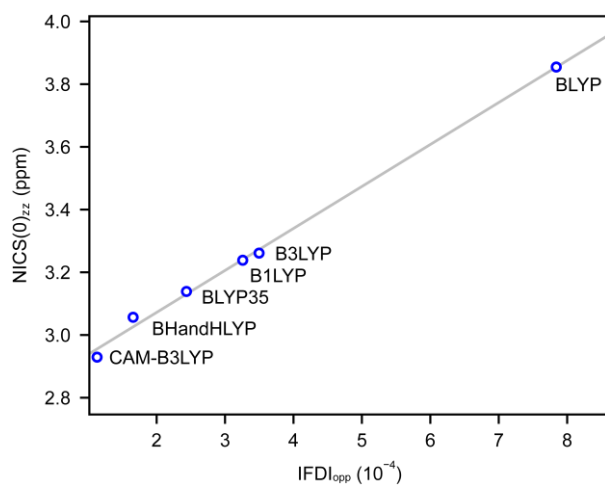
Figure S19 $IFDI_{opp}$ *vs* $NICS(0)_{zz}$ for neutral [8]CPP with different DFT functionals.
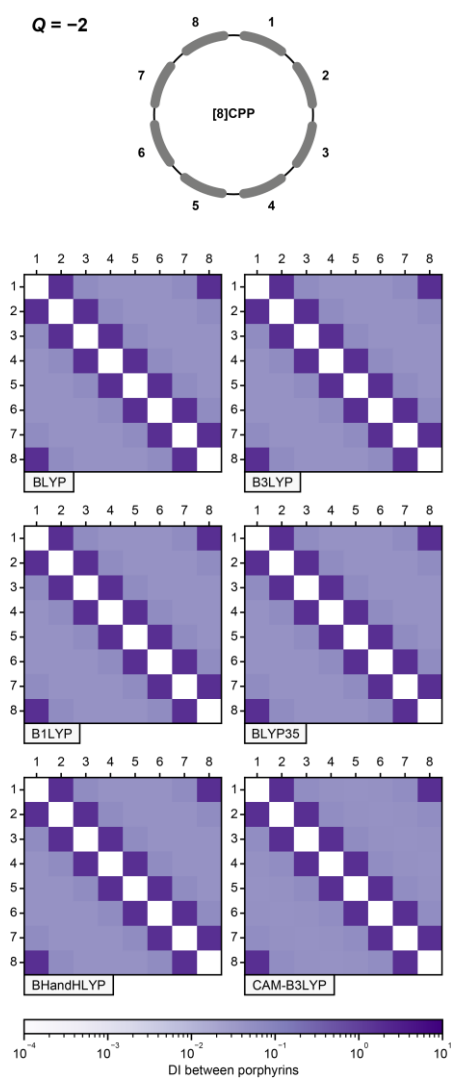
Figure S20 IFDI values between phenyl fragments in [8]CPP^{2-} with various DFT functionals.

S15
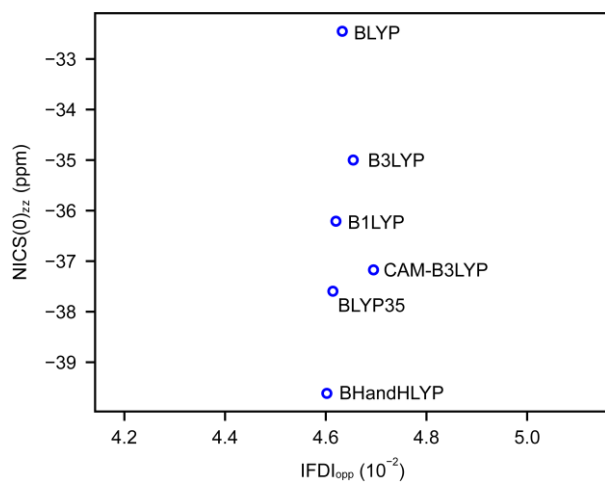
Figure S21 IFDI$_{opp}$ *vs* NICS(0)$_{zz}$ for [8]CPP^{2-} with different DFT functionals.
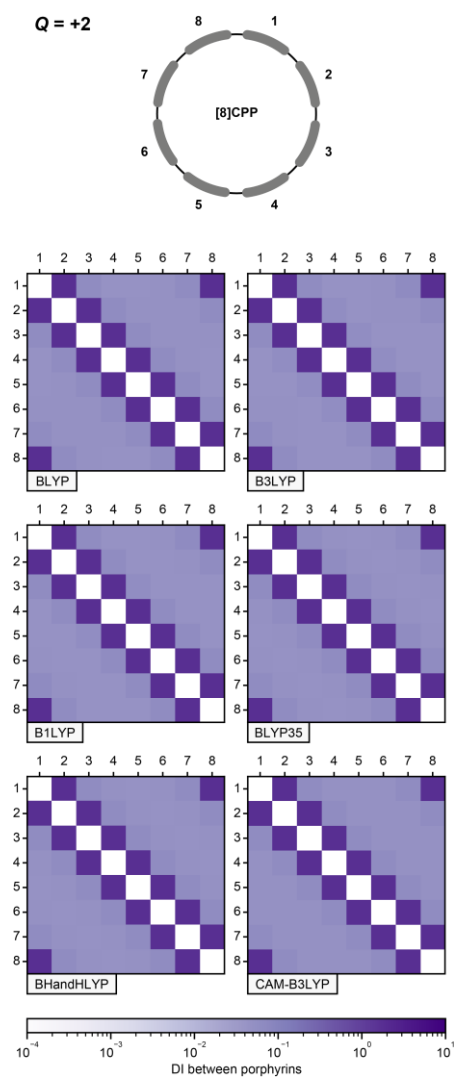
Figure S22 IFDI values between phenyl fragments in [8]CPP^{2+} using various DFT functionals.
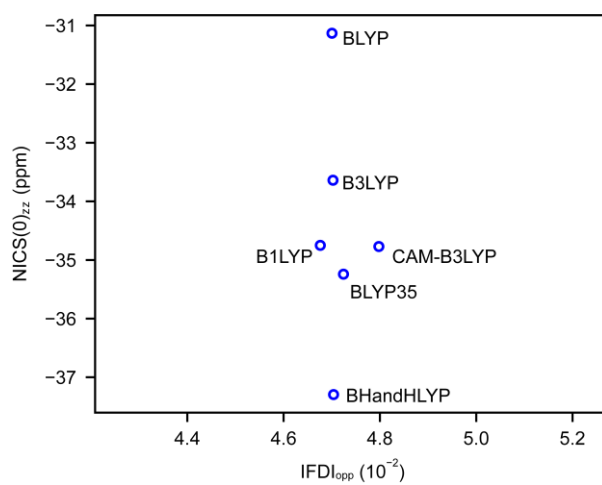
Figure S23 IFDI$_{opp}$ *vs* NICS(0)$_{zz}$ for [8]CPP^{2+} with different DFT functionals.
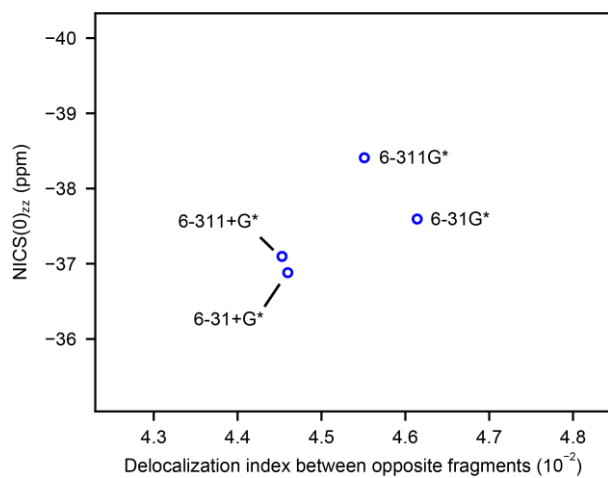
Figure S24 IFDI$_{opp}$ vs NICS(0)$_{zz}$ for [8]CPP^{2-} with different basis sets at the BLYP35 level. There is no appreciable difference between DI or NICS values when comparing different basis sets.

S6. Molecular orbital figures
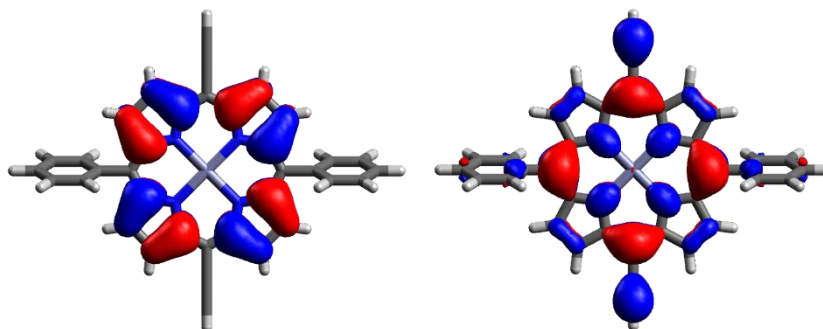
Figure S25 HOMO–1 (left) and HOMO (right) of a zinc porphyrin bisalkyne derivative calculated at the BLYP35/6-31G* level. Isosurfaces viewed in Avogadro with an isovalue of 0.02.

$Q = 0$, HOMO

$Q = +2$, HOMO (α) $Q = +2$, HOMO (β)
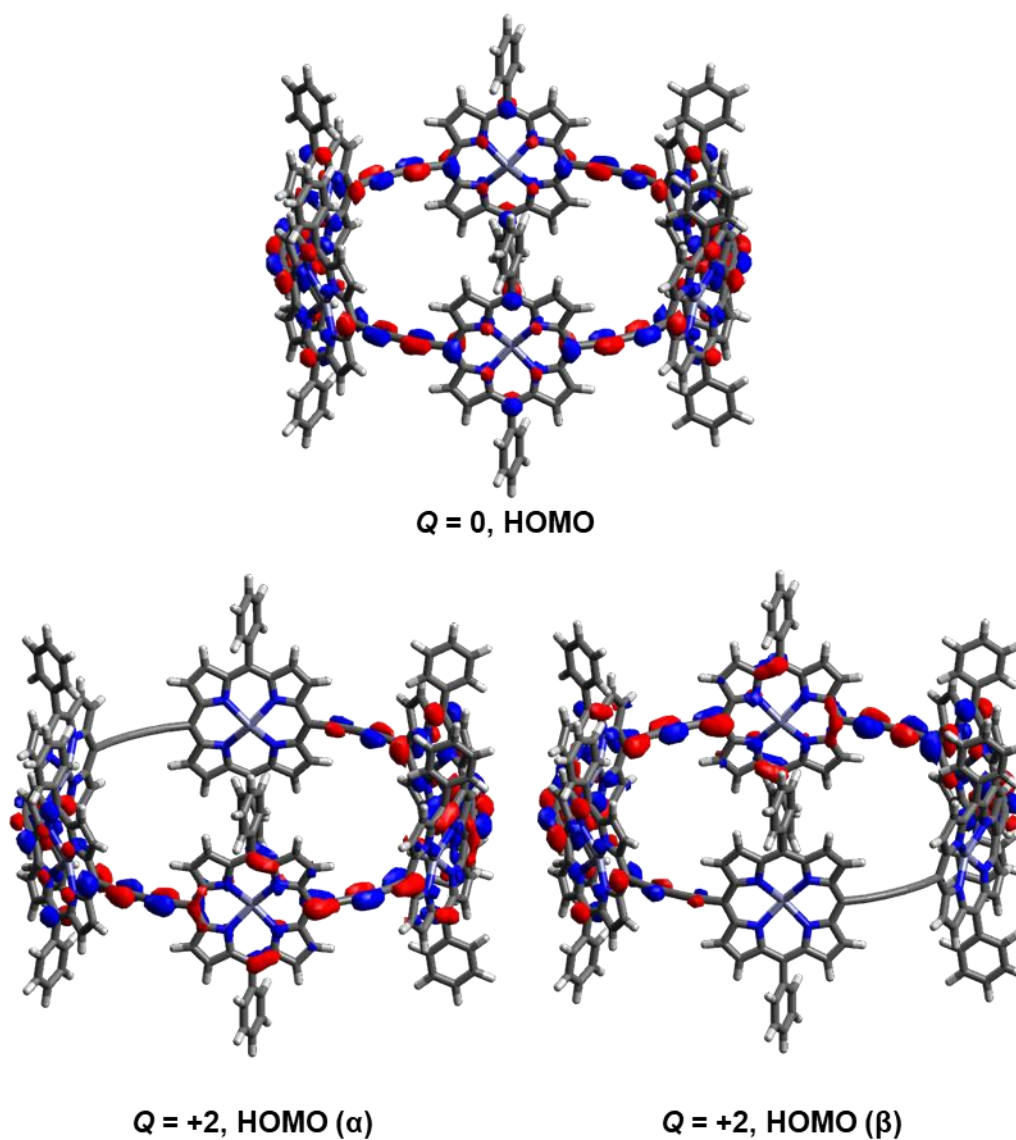
Figure S26 HOMOs of *c*-P6•T6^Q ($Q = 0, +2$) calculated at the BLYP35/6-31G* level. Isosurfaces visualized in Avogadro with an isovalue of 0.02. Template not displayed for clarity.

S7. Analysis of an acyclic nanoring

In order to investigate how much the delocalization indices are affected by oxidation, we performed calculations for an artificial model without cyclic conjugation, $\textbf{\textit{l}-P6•T6}^Q$, generated by removing one butadiyne link and replacing it with terminal hydrogen atoms (Figure S27). We have assigned the compound name $\textbf{\textit{l}-P6•T6}^Q$ to indicate that this model comprises a *linear* porphyrin hexamer (**\textit{l}-P6**) bound to the hexapyridyl template **T6**. For each oxidation state, the $IFDI_{opp}$ value for $\textbf{\textit{l}-P6•T6}^Q$ is around 34-72% of the value for $\textbf{\textit{c}-P6•T6}^Q$ (Table S2 and Figure S27, right): oxidation enhances electronic delocalization in both cyclic and acyclic models. A caveat of this analysis is that whereas the multiplicities of the tetra- and hexacations of **\textit{c}-P6·T6** are singlet, the $\textbf{\textit{l}-P6•T6}^Q$ models optimize to non-singlet wavefunctions. For this analysis, we treat the $\textbf{\textit{l}-P6•T6}^Q$ as a singlet (other than for $Q = +2$, which we treat as an open-shell singlet consistent with $\textbf{\textit{c}-P6•T6}^{2+}$).

Although $\textbf{\textit{l}-P6•T6}^Q$ exhibits appreciable delocalization, it is not a cyclic molecule and so it cannot be termed (anti)aromatic. Similarly, the average 3-bond separated DI in hexatriene is around 63% of benzene's PDI (Table S3), rising to 87% when the much lower $DI_{2,5}$ value is excluded; despite the fact that hexatriene has "high delocalization", it would not be considered aromatic since it is acyclic.

In order to assess the sensitivity of NMR chemical shifts to electronic delocalization *versus* aromaticity in the porphyrin nanoring, we calculated the chemical shifts of o_{in}, o_{out}, and template protons (Figure S29(b)) for both $\textbf{\textit{l}-P6•T6}^Q$ and $\textbf{\textit{c}-P6•T6}^Q$ (Figure S29 and Table S4). Table S4 shows chemical shift differences ($\Delta\delta$) for each resonance. For the template **T6** they are calculated as $\delta_{calc} - \delta_{ref}$, where δ_{ref} is the calculated chemical shift of a reference proton which is not subject to local or global shielding effects from a nanoring,[17] *i.e.* the chemical shift in the free (unbound) template **T6**. For protons o_{in} and o_{out} we use the difference ($o_{in} - o_{out}$), consistent with our previous work,[17] because this value is relatively selective for global ring current effects (where present). The data in Table S3 reveal that the $\Delta\delta$ values change upon oxidation for both **\textit{l}-P6•T6** and **\textit{c}-P6•T6**, but whereas for **\textit{l}-P6•T6** the variation is roughly monotonic and proportional to the charge on the ring (Q), for **\textit{c}-P6•T6** there is an additional component for $Q = +2$, +4 and +6, which we attribute to global ring current effects. This result is illustrated in Figure S29, which shows the difference in $\Delta\delta$ values between linear and cyclic molecules ($\Delta\Delta\delta = \Delta\delta(\textbf{\textit{l}-P6•T6}) - \Delta\delta(\textbf{\textit{c}-P6•T6})$). For $Q = 0$ and $Q = +12$, the $\Delta\Delta\delta$ values are approximately zero: in other words, the chemical shifts are scarcely affected by whether the molecule is cyclic, as would be expected in the absence of global aromaticity. In contrast, the $Q = +2$, +4, and +6 oxidation states have significant $\Delta\Delta\delta$ values, illustrating that cyclization is linked to a change of the NMR spectrum in these (putatively (anti)aromatic) states. The $\Delta\Delta\delta$ values for each state are approximately proportional its global ring current strength (main text Figure 2).
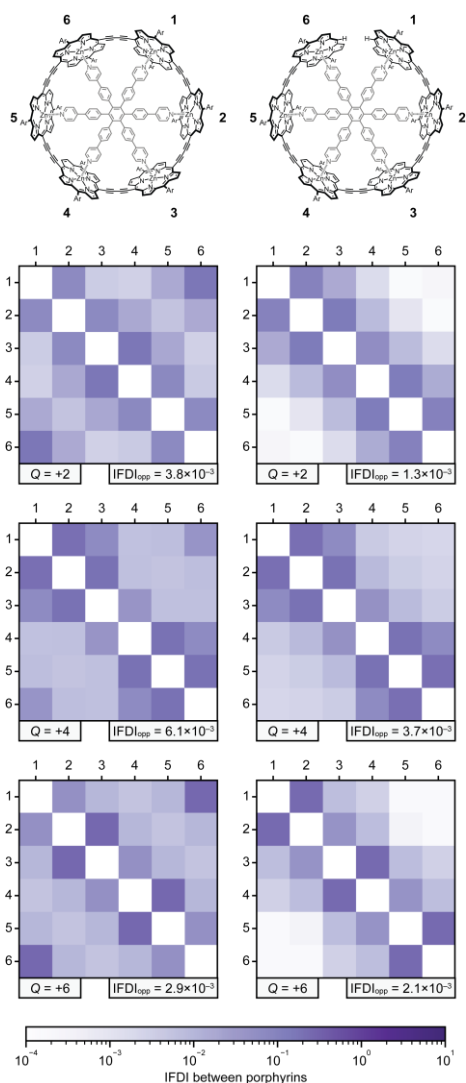
Figure S27 Matrices of IFDI values between fragments in **c-P6•T6**^{Q} (left column), and an acyclic model **l-P6•T6**^{Q} where one butadiyne bridge was removed. The mean IFDI between opposite porphyrins is reported as IFDI$_{opp}$. Calculated at the BLYP35/6-31G* level.

Table S2 Interfragment delocalization indices (IFDI$_{opp}$) for **c-P6•T6**^{Q} and the acyclic model **l-P6•T6**^{Q}. Calculated at the BLYP35/6-31G* level.

	IFDI$_{opp}$	
Q	**c-P6•T6**^{Q}	**l-P6•T6**^{Q}
0	9.5×10^{-5}	5.6×10^{-5}
+2	3.8×10^{-3}	1.3×10^{-3}
+4	6.1×10^{-3}	3.7×10^{-3}
+6	2.9×10^{-3}	2.1×10^{-3}
+12	7.0×10^{-8}	4.0×10^{-8}
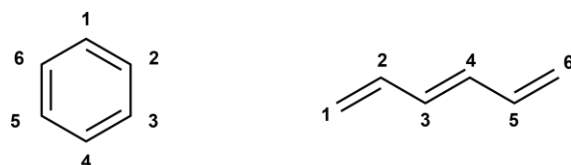
Figure S28 Carbon atom labels for DI/PDI calculations.

Table S3 Delocalization indices between *para* positions in benzene, and between carbon atoms which are separated by three bonds in hexatriene. See **Figure S28** for atom numbering. Calculated at the BLYP35/6-31G* level.

	$1-4$	$2-5$	$3-6$	PDI
benzene	0.1039	0.1039	0.1039	0.1039
hexatriene	0.0906	0.0150	0.0906	n.d.
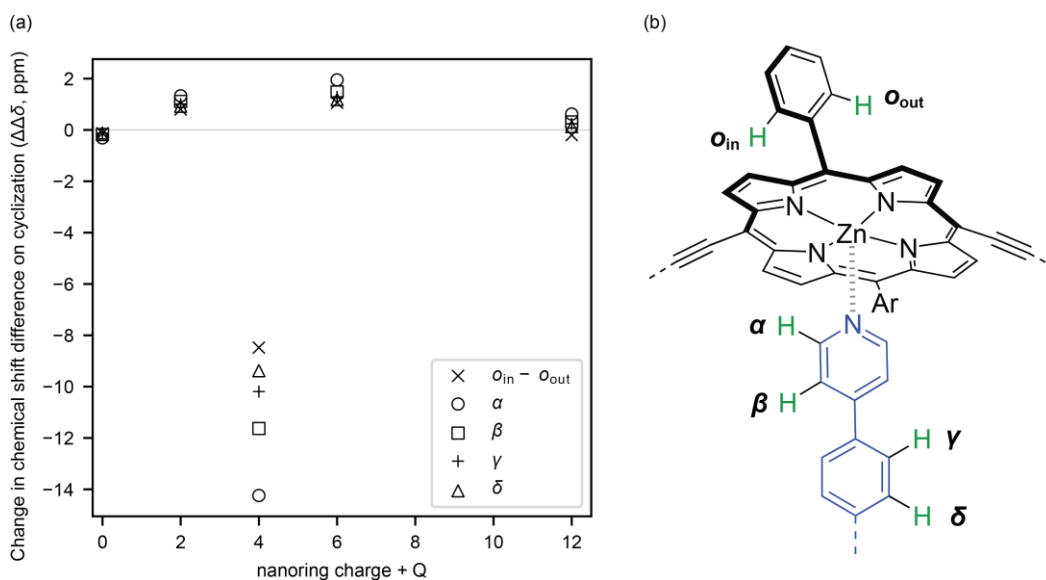
Figure S29: (a) Comparison of changes in chemical shift differences between acyclic (*l*-P6•T6) and cyclic (*c*-P6•T6) nanoring models as a function of charge; (b) labelled fragment of a nanoring showing proton assignments.

Table S4 Comparison of Δδ (ppm) values between a fully globally-conjugated porphyrin (*c*-P6•T6) nanoring and an acyclic nanoring (*l*-P6•T6) in which a single butadiyne bridge has been replaced with two hydrogen atoms. Calculated at the BLYP35/6-31G* level.

		$\delta(o_{(in)}) - \delta(o_{(out)})$	$\Delta\delta(\alpha)$	$\Delta\delta(\beta)$	$\Delta\delta(\gamma)$	$\Delta\delta(\delta)$
Q = 0	*l*-P6•T6^Q	0.31	−6.10	−2.49	−1.89	−1.56
	c-P6•T6^Q	0.44	−5.79	−2.31	−1.76	−1.44
Q = +2	*l*-P6•T6^Q	0.24	−4.36	−1.76	−1.37	−1.13
	c-P6•T6^Q	−0.56	−5.69	−2.87	−2.38	−2.05
Q = +4	*l*-P6•T6^Q	0.07	−2.16	−0.82	−0.71	−0.57
	c-P6•T6^Q	8.55	12.08	10.81	9.48	8.81
Q = +6	*l*-P6•T6^Q	−0.12	−0.04	0.11	−0.05	−0.02
	c-P6•T6^Q	−1.18	−1.99	−1.37	−1.34	−1.20
Q = +12	*l*-P6•T6^Q	−1.73	3.71	1.96	1.31	1.09
	c-P6•T6^Q	−1.53	3.09	1.65	1.07	0.96

S8. References

1 M. J. Frisch, G. W. Trucks, H. B. Schlegel, G. E. Scuseria, M. A. Robb, J. R. Cheeseman, G. Scalmani, V. Barone, G. A. Petersson, H. Nakatsuji, X. Li, M. Caricato, A. V. Marenich, J. Bloino, B. G. Janesko, R. Gomperts, B. Mennucci, H. P. Hratchian, J. V. Ortiz, A. F. Izmaylov, J. L. Sonnenberg, Williams, F. Ding, F. Lipparini, F. Egidi, J. Goings, B. Peng, A. Petrone, T. Henderson, D. Ranasinghe, V. G. Zakrzewski, J. Gao, N. Rega, G. Zheng, W. Liang, M. Hada, M. Ehara, K. Toyota, R. Fukuda, J. Hasegawa, M. Ishida, T. Nakajima, Y. Honda, O. Kitao, H. Nakai, T. Vreven, K. Throssell, J. A. Montgomery Jr., J. E. Peralta, F. Ogliaro, M. J. Bearpark, J. J. Heyd, E. N. Brothers, K. N. Kudin, V. N. Staroverov, T. A. Keith, R. Kobayashi, J. Normand, K. Raghavachari, A. P. Rendell, J. C. Burant, S. S. Iyengar, J. Tomasi, M. Cossi, J. M. Millam, M. Klene, C. Adamo, R. Cammi, J. W. Ochterski, R. L. Martin, K. Morokuma, O. Farkas, J. B. Foresman and D. J. Fox, Gaussian 16 2016.

2 M. Renz, M. Kess, M. Diedenhofen, A. Klamt and M. Kaupp, *J. Chem. Theor. Comput.*, 2012, **8**, 4189–4203.

3 A. D. Becke, *Phys. Rev. A*, 1988, **38**, 3098–3100.

4 C. Lee, W. Yang and R. G. Parr, *Phys. Rev. B*, 1988, **37**, 785–789.

5 C. Adamo and V. Barone, *Chem. Phys. Lett.*, 1997, **274**, 242–250.

6 R. Ditchfield, W. J. Hehre and J. A. Pople, *J. Chem. Phys.*, 1971, **54**, 724–728.

7 W. J. Hehre, R. Ditchfield and J. A. Pople, *J. Chem. Phys.*, 1972, **56**, 2257–2261.

8 P. C. Hariharan and J. A. Pople, *Theoret. Chim. Acta*, 1973, **28**, 213–222.

9 V. A. Rassolov, J. A. Pople, M. A. Ratner and T. L. Windus, *J. Chem. Phys.*, 1998, **109**, 1223–1229.

10 T. M. Henderson, A. F. Izmaylov, G. Scalmani and G. E. Scuseria, *J. Chem. Phys.*, 2009, **131**, 044108.

11 T. Yanai, D. P. Tew and N. C. Handy, *Chem. Phys. Lett.*, 2004, **393**, 51–57.

12 I. Casademont-Reig, R. Guerrero-Avilés, E. Ramos-Cordoba, M. Torrent-Sucarrat and E. Matito, *Angew. Chem. Int. Ed.*, 2021, **60**, 24080–24088.

13 A. D. Becke, *J. Chem. Phys.*, 1993, **98**, 5648.

14 P. J. Stephens, F. J. Devlin, C. F. Chabalowski and M. J. Frisch, *J. Phys. Chem.*, 1994, **98**, 11623–11627.

15 Y. Zhao and D. G. Truhlar, *Theor. Chem. Acc.*, 2008, **120**, 215–241.

16 S. Grimme, J. Antony, S. Ehrlich and H. Krieg, *J. Chem. Phys.*, 2010, **132**, 154104.

17 D. Bradley, M. Jirásek, H. L. Anderson and M. D. Peeks, *Chem. Sci.*, 2023, **14**, 1762–1768.

18 T. Lu and F. Chen, *J. Comp. Chem.*, 2012, **33**, 580–592.

19 AIMAll (Version 19.10.12), Todd A. Keith, TK Gristmill Software, Overland Park KS, USA, 2019 (aim.tkgristmill.com).